

Learning to Stylize Novel Views

Hsin-Ping Huang¹, Hung-Yu Tseng¹, Saurabh Saini², Maneesh Singh², Ming-Hsuan Yang^{1,3,4}

¹UC Merced ²Verisk Analytics ³Google Research ⁴Yonsei University

https://hhsinping.github.io/3d_scene_stylization

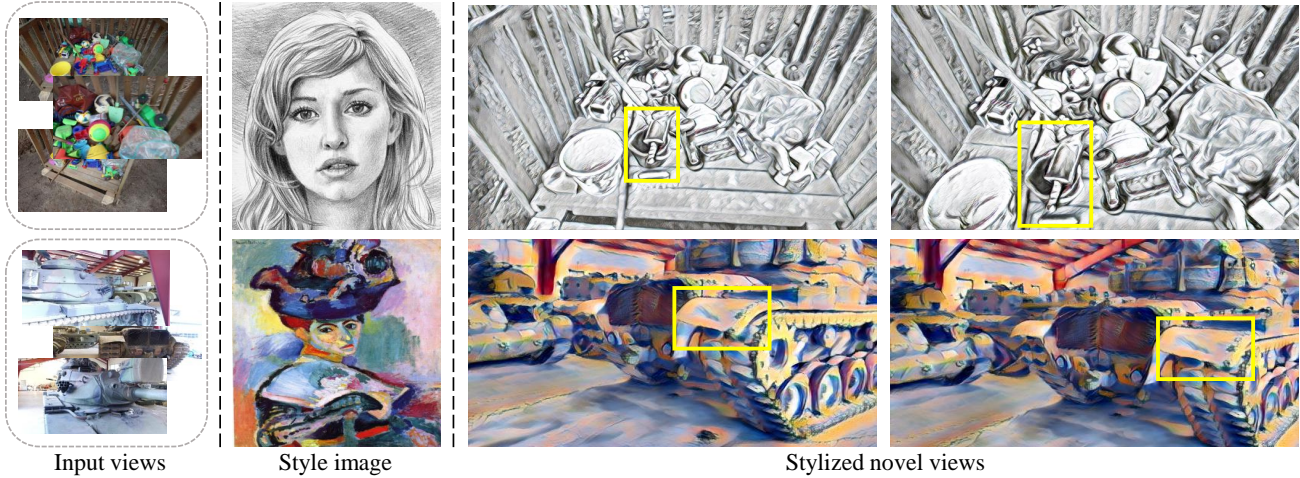


Figure 1. **3D scene stylization.** Given a set of images of a 3D scene (*left*) as well as a reference image of the desired style (*middle*), our method is able to modify the style of the 3D scene, and synthesize images of arbitrary novel views (*right*). The novel view synthesis results 1) contain the desired style and 2) are consistent across various novel views, *e.g.* the texture in the yellow boxes.

Abstract

We tackle a 3D scene stylization problem — generating stylized images of a scene from arbitrary novel views given a set of images of the same scene and a reference image of the desired style as inputs. Direct solution of combining novel view synthesis and stylization approaches lead to results that are blurry or not consistent across different views. We propose a point cloud-based method for consistent 3D scene stylization. First, we construct the point cloud by back-projecting the image features to the 3D space. Second, we develop point cloud aggregation modules to gather the style information of the 3D scene, and then modulate the features in the point cloud with a linear transformation matrix. Finally, we project the transformed features to 2D space to obtain the novel views. Experimental results on two diverse datasets of real-world scenes validate that our method generates consistent stylized novel view synthesis results against other alternative approaches.

1. Introduction

Visual content creation in 3D space has recently attracted increasing attention. Driven by the success of 3D scene representation approaches [59, 81, 113], recent methods make

significant progress on various content creation tasks for 3D scenes, such as semantic view synthesis [27, 30] and scene extrapolation [50]. In this work, we focus on the 3D scene stylization problem. As shown in Figure 1, given a set of images of a target scene and a reference image of the desired style, our goal is to render stylized images of the scene from arbitrary novel views. 3D scene stylization enables a variety of interesting virtual reality (VR) and augmented reality (AR) applications, *e.g.* augment the street scene at user locations to the *Cafe Terrace at Night* style by van Gogh.

Learning to modify the style of an existing 3D scene is challenging for two reasons. First, the synthesized novel views (*i.e.* 2D images) of the stylized 3D scene must contain the desired style provided by the reference image. Second, since our goal is to stylize the *holistic* 3D scene, the generated novel views need to be consistent across different viewpoints for the same scene, such as the texture in the yellow boxes shown in Figure 1.

To handle these challenges, one plausible solution is to combine existing novel view synthesis [81, 113] and image stylization approaches [44, 92]. However, such straightforward approaches lead to problematic results since image stylization schemes are not designed to consider the consistency issue across different views for the same scene.

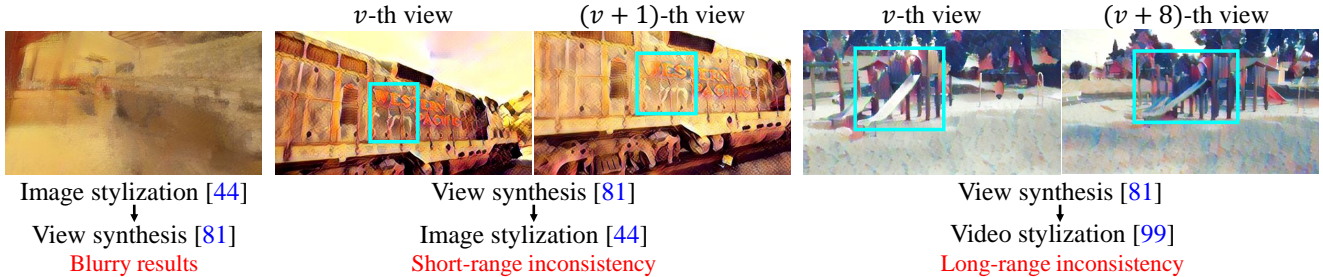


Figure 2. **Motivation.** While the existing methods can be used for the 3D scene stylization task, these methods either produce blurry (image stylization \rightarrow novel view synthesis), short-range inconsistent (novel view synthesis \rightarrow image stylization), or long-range inconsistent (novel view synthesis \rightarrow video stylization) results.

We present the examples in Figure 2 where the results may be blurry if the input images of the target scene are stylized before conducting novel view synthesis. On the other hand, if we apply image stylization after novel view synthesis, the results are not consistent across different views. Another possible solution is to treat a series of novel view synthesis results as a *video*, and use the video stylization frameworks [14, 20, 99] to obtain temporally consistent results. However, as shown in Figure 2, these approaches are not able to enforce long-range consistency (*i.e.* between two far-away views) as the video stylization schemes only guarantee the short-term consistency.

In this paper, we propose a point cloud-based method for consistent 3D scene stylization. To synthesize novel views that 1) match *arbitrary* style images and 2) render images with consistent appearance across different views, the core idea is to operate on the 3D scene representation, *i.e.* point cloud, of the target scene. Given a set of input images of the target scene, we first construct the point cloud by back-projecting the image features to the 3D space according to the pre-computed 3D proxy geometry. To transfer the style of the holistic 3D scene, we develop a point cloud transformation module. Specifically, we use a series of point cloud aggregation modules to gather the style information of the 3D scene. We then modulate the features in the point cloud with a linear transformation matrix [44] computed according to the style information of the point cloud and reference image. Finally, we project the transformed features from the point cloud to the 2D space to obtain the novel view synthesis results. Since our method synthesizes novel view images from the same stylized point cloud, the rendered results not only demonstrate the desired style, but also are consistent across different viewpoints.

We evaluate the proposed 3D scene stylization method through extensive qualitative and quantitative studies. The experiments are conducted on two diverse datasets of real-world scenes: Tanks and Temples [37] and FVS [80]. We conduct a user preference study to evaluate the stylization quality, *i.e.* whether the novel view synthesis results match the style of the reference image. In addition, we use the Learned Perceptual Image Patch Similarity (LPIPS) [114] metric to measure the consistency of the results synthesized

across different novel views.

We make the following contributions in this paper:

- We propose a point cloud-based framework for the 3D scene stylization task.
- We design a point cloud transformation module that learns to transfer the style from an arbitrary 2D reference image to the point cloud of a 3D scene.
- We validate that our method produces high-quality and consistent stylized novel view synthesis results on the Tanks and Temples as well as FVS datasets.

2. Related Work

Novel View Synthesis. Given a set of images for a scene, novel view synthesis aims to generate high-quality images at arbitrary viewpoints. It can be categorized by the number of input images that cover the scene. One line of work takes as input a single image or stereo images. These methods use multi-plane images [89, 96, 103, 118], layer depth image [39, 86], or point cloud [64, 102] representations to synthesize images at novel views near the input views, *e.g.* 3D photo. To enable the image synthesis at *arbitrary* novel views, several recent frameworks take hundreds of input images of a scene as the input. These frameworks leverage different 3D representations to accomplish the task. Image-based rendering approaches [80, 81] compute 3D proxy geometry of the scene, and generate images by warping the input frames to the desired novel views. Neural radiance field schemes [51, 59, 112, 113] use multi-layer perceptrons to implicitly encode the scene for novel view synthesis. Point cloud-based methods [57, 1] solve different optimization problems to construct the point cloud for a specific 3D scene. Different from these frameworks, our goal is to generate *stylized* novel view images of the 3D scene. As shown in Figure 2, while existing algorithms can be used for the 3D scene stylization task, they fail to generate high-quality novel view synthesis results with the desired style.

Image and Video Stylization. Image stylization [22] aims to transfer the style of a reference image to the single input image. Existing methods [9, 33, 46, 85, 97] are designed based on feed-forward networks for transferring a set of *pre-defined* styles. For *arbitrary* image style transfer,

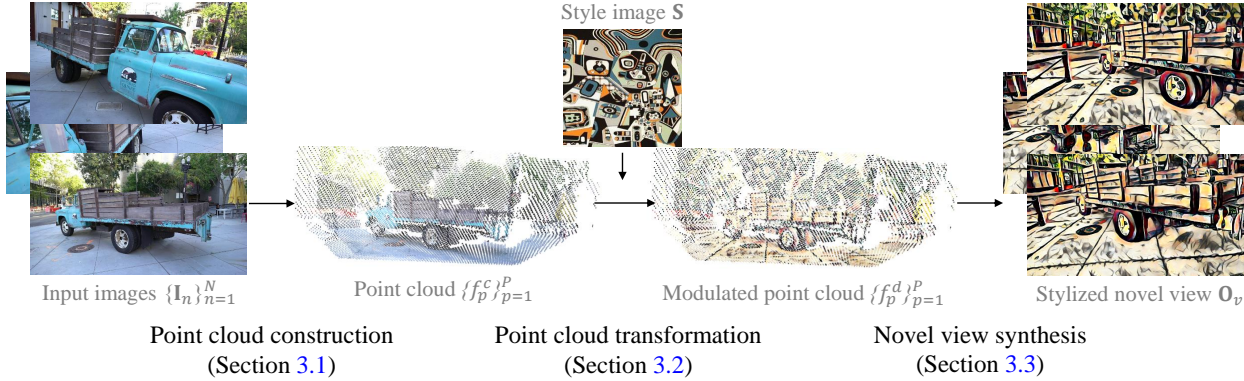


Figure 3. **Algorithmic overview.** The proposed method consists of three steps: 1) constructing the 3D point cloud from the set of input images $\{\mathbf{I}_n\}_{n=1}^N$, 2) transforming the point cloud according to the reference image \mathbf{S} with the desired style, and 3) synthesizing the stylized image \mathbf{O}_v at arbitrary novel view v . The coloring of the point clouds is for visualization purposes only. In our approach, the point clouds store the features rather than RGB values.

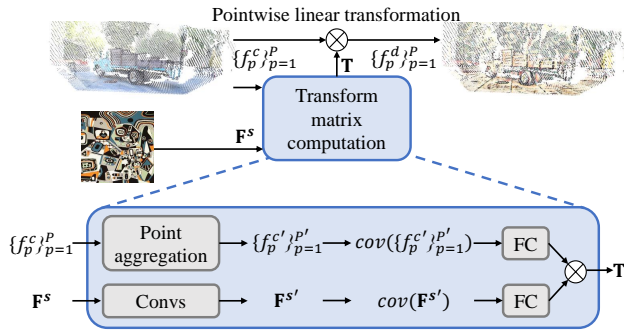


Figure 4. **Point cloud transformation.** We model the 3D scene stylization process as the linear transformation between the constructed and stylized point clouds. Specifically, the constructed point cloud is modulated using the predicted linear transformation matrix \mathbf{T} , as described in (1). We use a series of point cloud aggregation modules to gather the point cloud information, and the convolution layers to process the reference image feature \mathbf{F}^s to compute the matrix \mathbf{T} .

Huang and Belongie [31] use first-order statistics to encode the style information, and transform the image style via the AdaIN normalization layers. The WCT [47] approach uses whitening and coloring transformation to match the second-order statistics of the input image to those of the reference image. In addition, the LST [44] scheme leverages the convolutional neural networks to reduce the computational cost of solving the transformation matrix in the WCT method for real-time universal style transfer. Most recently, the TPF method [92] proposes a regularization layer to facilitate the generalization of image stylization models.

Video stylization aims to transfer the style of a reference image to a sequence of video frames. To address the temporal flickering issue produced by the image stylization approaches, numerous approaches [8, 11, 18, 26, 29] incorporate optical flow modules to train feed-forward networks for transferring a particular style to the videos. Several recent frameworks [14, 20, 99] enable the video style trans-

fer to *arbitrary* styles. Although significant advances have been made, existing methods are designed specifically for transferring the style of 2D images or video sequences. As shown in Figure 2, simply applying these schemes for the 3D scene stylization task leads to problematic results, such as blurry or short/long-range inconsistent images across different novel views.

Several efforts have been made to perform the stylization in 3D space. However, these approaches are only applicable to single objects [34], narrow-baseline stereo images [10, 23], or light field images [28]. In contrast, our method stylizes complex 3D scenes, and produces consistent results at arbitrary viewpoints.

Deep neural networks for point clouds. Various deep neural network (DNN)-based models [36, 41, 42, 45, 72, 73, 104, 108, 116] that take point clouds as input are widely studied for vision recognition tasks including 3D semantic segmentation [2], 3D shape classification or normal estimation [105], and 3D object part segmentation [110]. Recently, Mallya *et al.* [54] proposes a point cloud colorization approach for the video-to-video synthesis task. In this work, we propose a DNN-based point cloud transformation model for the 3D scene stylization task. We note that the PSNet [5] model aims to transfer the style of the point cloud. Nevertheless, there are two issues for the PSNet method to be applied to the 3D scene stylization task. First, it does not support synthesizing high-quality stylized images at novel views, which makes the PSNet framework limited for real-world (*e.g.* AR) applications. Second, since the PSNet scheme requires the optimization process for each specific scene, it is time-consuming, and fails to handle large-scale scenes in the real-world with more than 60M points, such as those in the Tanks and Temples dataset [37]. In contrast, we propose a feed-forward point cloud model that is efficient, capable of handling large-scale 3D scenes, and generating images with arbitrary styles at various novel views.

3. Methodology

We present the overview of the proposed 3D scene stylization framework in Figure 3. Given a set of N input images $\{\mathbf{I}_n\}_{n=1}^N$ of a static scene, and a reference image \mathbf{S} with the desired style, our goal is to synthesize the image \mathbf{O}_v at the novel view v with the camera pose (\mathbf{R}_v, t_v) and intrinsic \mathbf{K}_v . Specifically, the generated novel view image \mathbf{O}_v needs to 1) match the style of the reference image \mathbf{S} and 2) be consistent for different viewpoints v . To handle such (especially the consistency) requirements, our core idea is to 1) construct a single 3D representation, *i.e.* point cloud, for the holistic scene, and 2) transform the representation to produce not only stylized but also consistent novel view synthesis results. The proposed approach consists of three steps: point cloud creation, point cloud transformation, and novel view synthesis, described in the following sections.

3.1. Point Cloud Construction

Pre-processing. Our method leverages camera pose and proxy geometry to construct the 3D point cloud. Given the input images $\{\mathbf{I}_n\}_{n=1}^N$, we first use a structure-from-motion algorithm [82] to estimate the camera poses $\{\mathbf{R}_n, t_n\}_{n=1}^N$ and intrinsic parameters $\{\mathbf{K}_n\}_{n=1}^N$. For each image \mathbf{I}_n , we use the COLMAP [82, 84] and Delaunay-based reconstruction [32, 38] schemes to obtain the depth map \mathbf{D}_n that can appropriately back-project the points from the image plane to the 3D space.

Feature extraction and back-projection. Since our goal is to transform the point cloud representation for the 3D scene stylization purpose, we need the point cloud representation to encode the style information. Therefore, we use the VGG-19 model [87] pre-trained on the ImageNet [12] dataset to extract the relu3_1 feature maps $\{\mathbf{F}_n^c\}_{n=1}^N$ of the input images $\{\mathbf{I}_n\}_{n=1}^N$. The width and height of each feature map is H and W . According to the depth map $\{\mathbf{D}_n\}_{n=1}^N$, we back-project all the points in each feature map to build the 3D point cloud $\{f_p^c\}_{p=1}^P$, where $P = NHW$ is the total number of points in the constructed point cloud.

3.2. Point Cloud Transformation

We model the 3D scene stylization process as a linear transformation [44] between the constructed and stylized point clouds. Intuitively, the goal is to match the covariance statistics of the stylized point clouds and those of the reference image \mathbf{S} . To achieve this, we use the pre-trained VGG-19 network to extract the relu3_1 feature map from the reference image \mathbf{S} as the style feature map \mathbf{F}^s . Given the constructed point cloud $\{f_p^c\}_{p=1}^P$, we use a predicted linear transformation matrix \mathbf{T} to compute the modulated point cloud $\{f_p^d\}_{p=1}^P$, namely

$$f_p^d = \mathbf{T}(f_p^c - \bar{f}^c) + \bar{f}^s \quad \forall p \in [1, \dots, P], \quad (1)$$

where \bar{f}^c is the mean of the features in the point cloud $\{f_p^c\}_{p=1}^P$, and \bar{f}^s is the mean of the style feature map \mathbf{F}^s .

Linear transformation matrix \mathbf{T} . The transformation matrix \mathbf{T} is computed from the style feature map \mathbf{F}^s and constructed point cloud $\{f_p^c\}_{p=1}^P$. As shown in Figure 4, we adopt the strategy similar to the LST [44] method that uses the convolution layers, covariance computation, and fully-connected layers to compute the matrix \mathbf{T}^s from the style feature map \mathbf{F}^s . On the other hand, we develop a series of point cloud aggregation modules to process the point cloud $\{f_p^c\}_{p=1}^P$, and use the covariance computation followed by the fully-connected layers to calculate the matrix \mathbf{T}^c . Finally, we obtain the transformation matrix $\mathbf{T} = \mathbf{T}^s \mathbf{T}^c$.

Point cloud aggregation. It is challenging to gather the information contained in the constructed point cloud $\{f_p^c\}_{p=1}^P$ due to the sparsity and non-uniformity. We note that the constructed point cloud is non-uniform if the input images cover a particular region of the 3D scene. In this work, we leverage the set abstraction [74] concept to aggregate the point cloud. The input $\{f_p^c\}_{p=1}^P$ to a point cloud aggregation module is a set of P points with feature dimension c , and the output $\{f_p^{c'}\}_{p=1}^{P'}$ is a set of P' points with dimension c' . We first sample a subset of P' points $\{f_p^c\}_{p=1}^{P'}$ using the iterative farthest point sampling algorithm [24, 60]. Viewing the sampled points as the centroids in the 3D space, we use a radius parameter r to find the nearby points to form a point group. By using the MLP layers and the max pooling operator to map each point group to a vector, we obtain the aggregated point cloud $\{f_p^{c'}\}_{p=1}^{P'}$. The output $\{f_p^{c'}\}_{p=1}^{P'}$ is then used as the input for the next module. We use three point cloud aggregation modules sequentially in our pipeline.

3.3. Novel View Synthesis and Model Training

We aim to synthesize stylized image \mathbf{O}_v at an arbitrary novel view v . Given the target camera pose (\mathbf{R}_v, t_v) and intrinsic \mathbf{K}_v , we use Pytorch3D [76, 102] to render the transformed 2D feature map \mathbf{F}_v^d . We then use a decoder network to generate the stylized novel view image \mathbf{O}_v from the 2D feature map \mathbf{F}_v^d .

Model training. We keep the pre-trained VGG-19 feature extractor fixed during the whole training phase. We first train the decoder network to perform the non-stylized novel view synthesis. Since the ground-truth (non-stylized) novel view image is available in the training sets, we use the ℓ_1 reconstruction loss to optimize the decoder network. We then keep the decoder network fixed, and train the proposed point cloud transformation module with the following loss functions:

- **Content loss \mathcal{L}_c** ensures the preservation of the content information by measuring the distance between the pre-trained VGG-19 features of the generated stylized image \mathbf{O}_v and the ground-truth (non-stylized) image \mathbf{I}_v .
- **Style loss \mathcal{L}_s** encourages the synthesized image \mathbf{O}_v

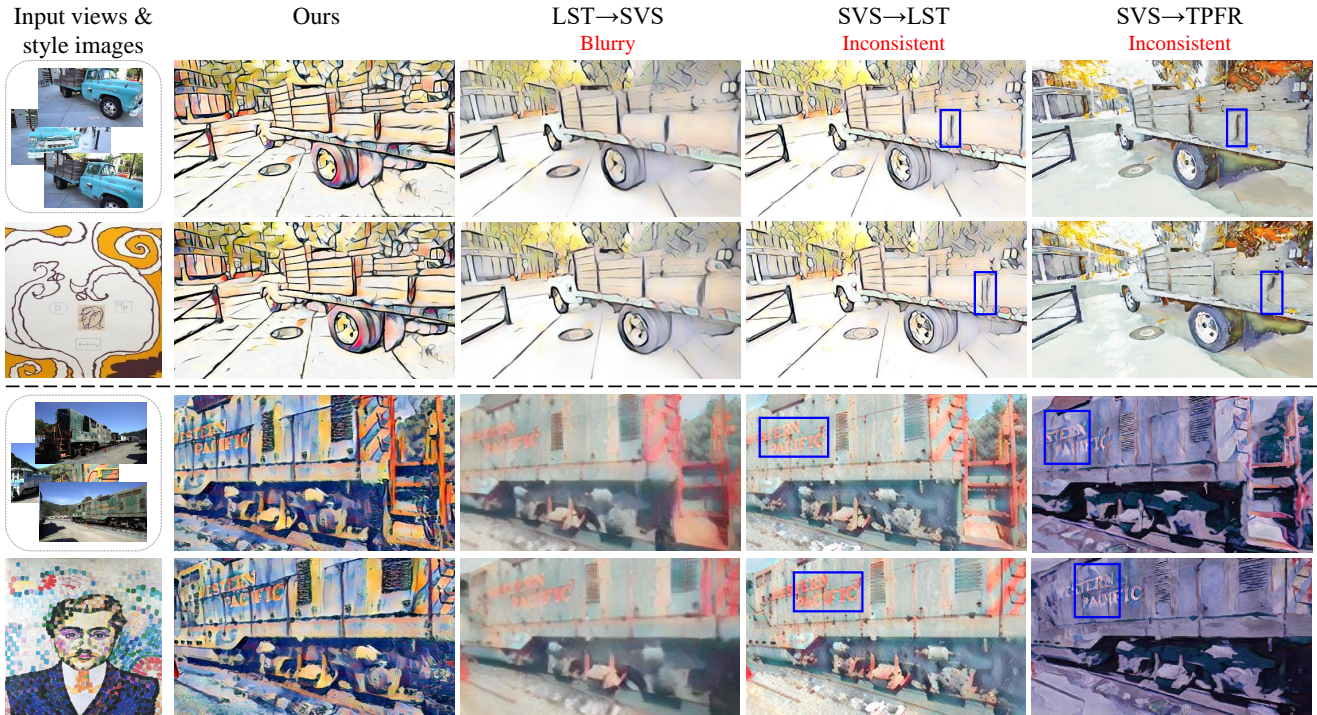


Figure 5. **Visual comparisons to image stylization-based approaches.** We compare the stylized novel view images generated by the three image stylization alternative schemes and our model on Tanks and Temples dataset [37].

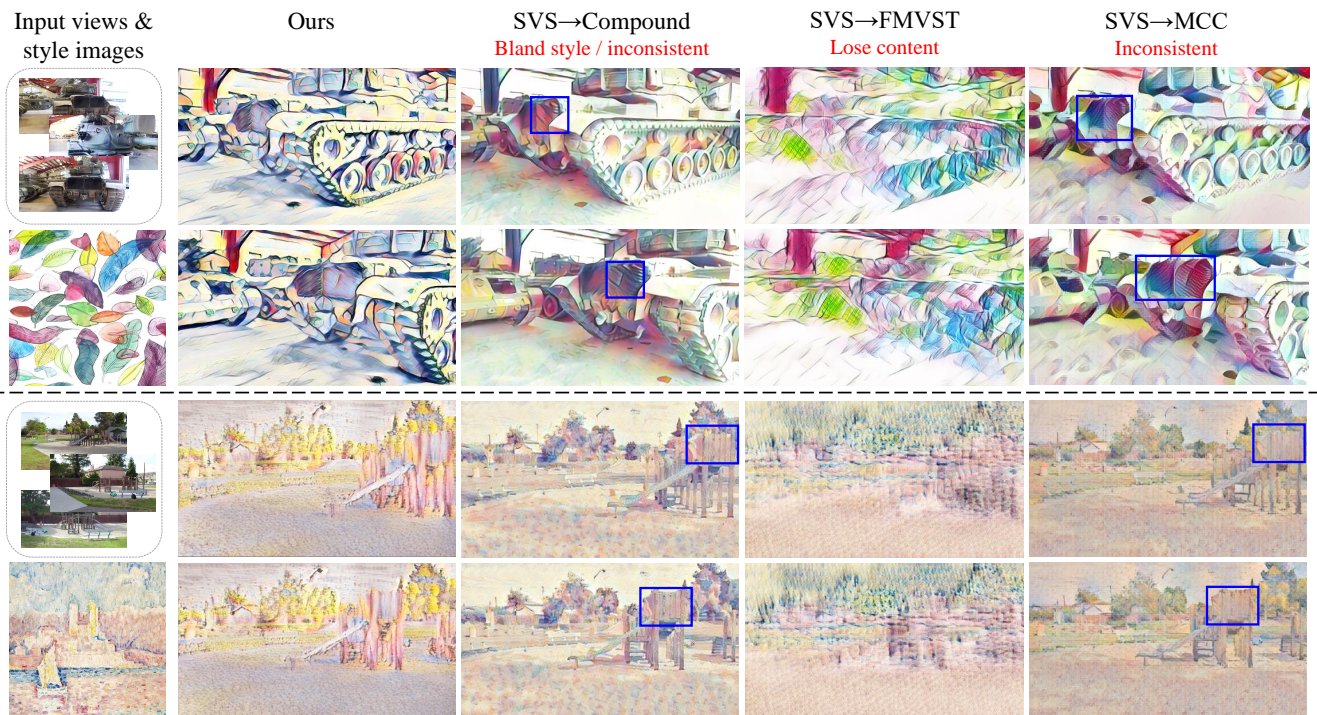


Figure 6. **Visual comparisons to video stylization-based approaches.** We compare the stylized novel view images generated by the three video stylization alternative schemes and our model on Tanks and Temples dataset [37].

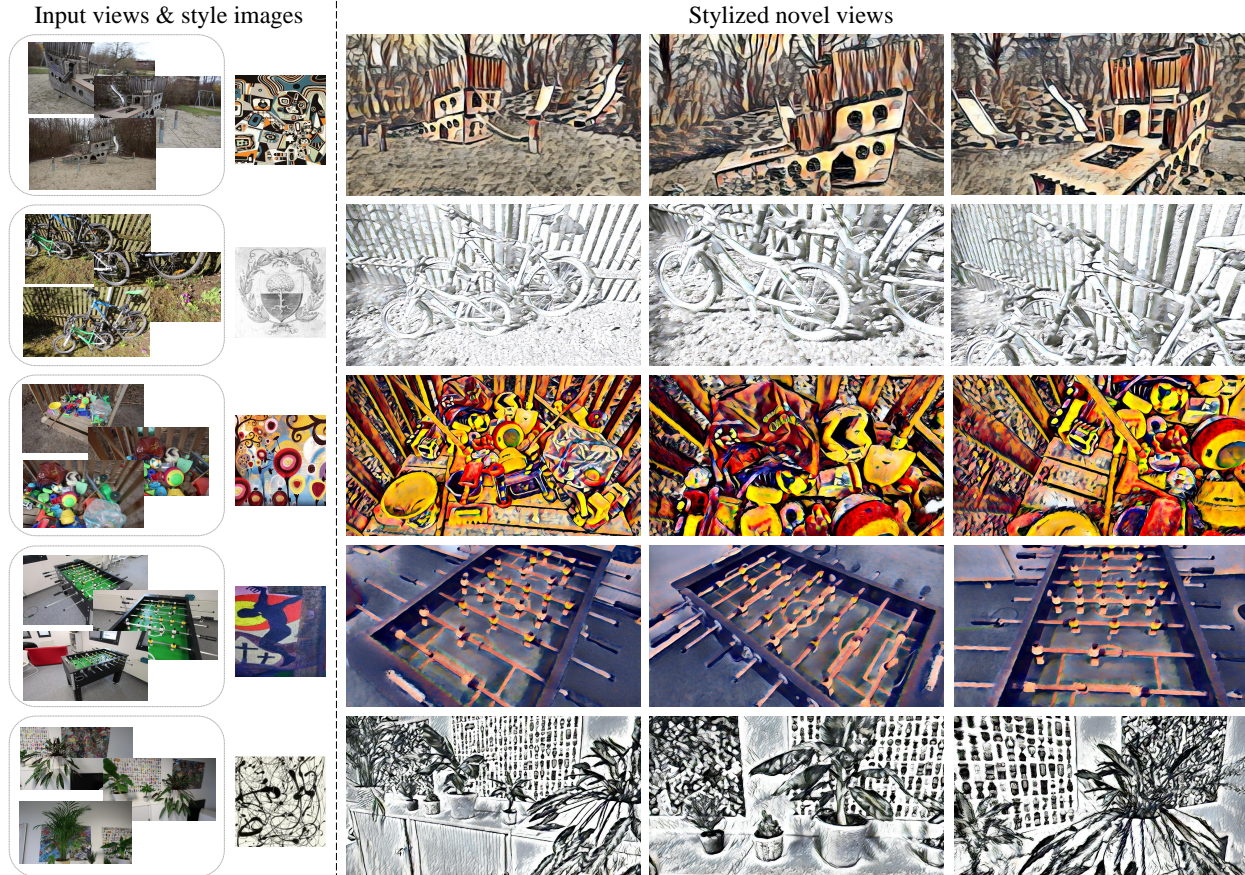


Figure 7. **Qualitative results on the FVS dataset.** We demonstrate the generalization of the proposed approach by training on the Tanks and Temples dataset, then testing on the FVS dataset.

to match the style of the reference image \mathbf{S} . Similar to recent style transfer approaches [33, 44], we extract the features at different layers of the pre-trained VGG-19 model, and compute the gram matrix differences.

The overall loss function for training the point cloud transformation module is

$$\mathcal{L} = \mathcal{L}_c(\mathbf{O}_v, \mathbf{I}_v) + \lambda \mathcal{L}_s(\mathbf{O}_v, \mathbf{S}), \quad (2)$$

where λ controls the importance of each loss term.

4. Experimental Results

We conduct extensive experiments on two real-world datasets to validate the efficacy of the proposed 3D scene stylization model.

Datasets. We use the Tanks and Temples [37] dataset for quantitative evaluation. Similar to the setting in FVS [80], we use 17 out of the 21 scenes for the training. The four remaining scenes (Truck, Train, M60 and Playground) are used for testing. We also present qualitative results on the FVS [80] dataset, which consists of 6 scenes: Bike, Flowers, Pirate, Digger, Sandbox and Soccer table. Note that both datasets are collected by *handheld* cameras in un-

constraint motions.

Evaluated methods. As the 3D scene stylization task is a relatively new problem, we evaluate our method against alternative approaches built upon the state-of-the-art novel view synthesis NeRF++ [113], SVS [81], and image/video stylization schemes:

- **Image stylization** \rightarrow **novel view synthesis:** We first use image stylization schemes LST [44] or TPFR [92] to transfer the style to the input images $\{\mathbf{I}_n\}_{n=1}^N$, then perform novel view synthesis.
- **Novel view synthesis** \rightarrow **image stylization:** We apply image stylization to the novel view synthesis results.
- **Novel view synthesis** \rightarrow **video stylization:** We use a series of novel view synthesis results to create a *video*, then apply video stylization methods Compound [99], FMVST [20], or MCC [14].

4.1. Qualitative Results

Image stylization. Figure 5 presents the qualitative comparison between the stylized novel view images generated by the three image stylization alternative schemes and the proposed method. Since the images are stylized inde-

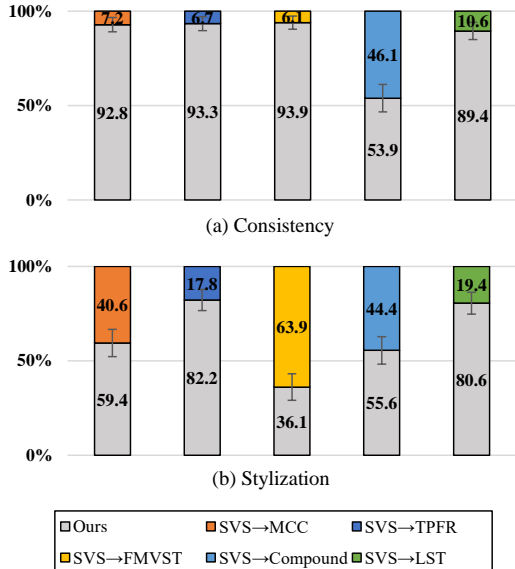


Figure 8. **User preference study.** We conduct a user study and ask subjects to select the results that (a) have more consistent contents across different video frames (e.g. less flickering), (b) better match the style of the example image. The number indicates the percentage of preference.

pendently without considering the consistency issue across different viewpoints, we observe two issues in the image stylization-based methods. First, LST \rightarrow SVS generally produces blurry novel view images. Since the stylized input images are not consistent, the novel view synthesis approach tends to *blend* such inconsistency, which leads to blurry results. Second, the novel view synthesis results are not consistent if we operate in the reverse order, i.e. SVS \rightarrow LST. We highlight the inconsistency using yellow boxes in Figure 5. Note that we observe the same problem if we replace SVS with NeRF++.

Video stylization. We qualitatively evaluate the results by the proposed method and three video stylization alternative approaches in Figure 6. Specifically, we create the videos using a series of novel view synthesis results. All the alternative approaches generate inconsistent results between two relatively far-away viewpoints since the video stylization methods only guarantee *short-term* consistency in the video. Although SVS \rightarrow Compound generates less inconsistent results, the style of the novel view images is bland and not aligned with that of the reference image. On the other hand, SVS \rightarrow FMVST creates images that better match the desired style, but fails to preserve the content of the original scene.

In contrast to the image and video stylization alternative approaches, our method 1) generates sharp novel view images with correct scene contents and the desired style, and 2) guarantees the short/long-range consistency. Furthermore, we demonstrate the generalization of the proposed

Table 1. **Short-range consistency.** We compare the long-range consistency using the warping error (\downarrow) between the viewpoints of $(t - 1)$ -th and t -th testing video frames in the Tanks and Temples dataset [37]. We report the average errors of 15 diverse styles. The best performance is in **bold** and the second best is underscored.

Method	Truck	Playground	Train	M60	Average
NeRF++ \rightarrow LST	0.215	0.168	0.250	0.274	0.231
SVS \rightarrow LST	0.192	0.159	0.220	0.241	0.206
NeRF++ \rightarrow TPFR	0.216	0.214	0.299	0.279	0.258
SVS \rightarrow TPFR	0.235	0.237	0.291	0.276	0.264
NeRF++ \rightarrow Compound	0.188	0.169	0.229	0.208	0.202
SVS \rightarrow Compound	0.166	0.156	<u>0.199</u>	0.160	<u>0.172</u>
NeRF++ \rightarrow FMVST	0.342	0.300	0.405	0.348	0.354
SVS \rightarrow FMVST	0.343	0.304	0.412	0.337	0.354
NeRF++ \rightarrow MCC	0.250	0.201	0.269	0.255	0.246
SVS \rightarrow MCC	0.242	0.198	0.260	0.224	0.232
Ours	<u>0.184</u>	<u>0.158</u>	0.170	<u>0.172</u>	0.170

Table 2. **Long-range consistency.** We compare the long-range consistency using the warping error (\downarrow) between the viewpoints of $(t - 7)$ -th and t -th testing video frames in the Tanks and Temples dataset [37]. We report the average errors of 15 diverse styles. The best performance is in **bold** and the second best is underscored.

Method	Truck	Playground	Train	M60	Average
NeRF++ \rightarrow LST	0.570	0.349	0.520	0.639	0.521
SVS \rightarrow LST	<u>0.567</u>	0.327	0.470	0.603	0.489
NeRF++ \rightarrow TPFR	0.579	0.436	0.503	0.655	0.541
SVS \rightarrow TPFR	0.605	0.430	0.470	0.581	0.513
NeRF++ \rightarrow Compound	0.586	0.398	0.477	0.557	0.498
SVS \rightarrow Compound	0.573	0.388	<u>0.422</u>	<u>0.460</u>	<u>0.449</u>
NeRF++ \rightarrow FMVST	0.742	0.525	0.636	0.695	0.644
SVS \rightarrow FMVST	0.732	0.519	0.620	0.662	0.626
NeRF++ \rightarrow MCC	0.691	0.450	0.535	0.646	0.571
SVS \rightarrow MCC	0.693	0.447	0.516	0.584	0.548
Ours	0.559	<u>0.337</u>	0.412	0.458	0.431

framework in Figure 7, where we use the model trained on the Tanks and Temples dataset to perform the 3D scene stylization task on the FVS dataset.

4.2. Quantitative Results

Stylization quality. We conduct a user study to understand the user preference between the proposed and the alternative approaches. For each testing scene in the Tanks and Temples dataset, we create a video using a series of stylized novel view synthesis results. By presenting two videos generated by different methods for the same scene, we ask the participants to select the one that (1) has more consistent contents across different video frames (e.g., less flickering), and (2) better matches the style of the reference image. As the results shown in Figure 8, the synthesized images by the proposed method are consistent and close to the reference style. We observe that the users slightly prefer the style generated by SVS \rightarrow FMVST. However, as illustrated in Section 4.1 and Figure 6, SVS \rightarrow FMVST fails to preserve the content of the original scene.

Short-range consistency. We use the warped LPIPS metric [114] to measure the consistency of the results across different viewpoints. Given a stylized image at a novel view

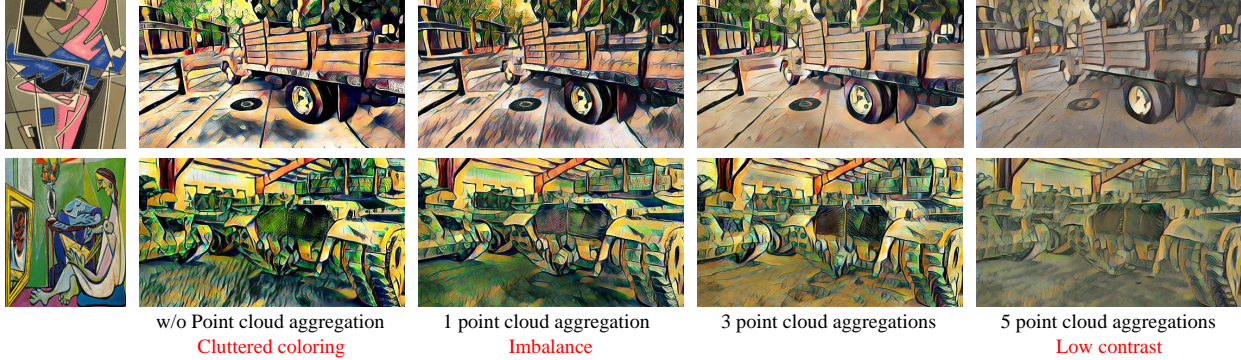


Figure 9. **Ablation study on the number of point cloud aggregation modules.** We compare the visual results of using 0/1/3/5 modules. We empirically decide to use 3 modules for better visual quality.

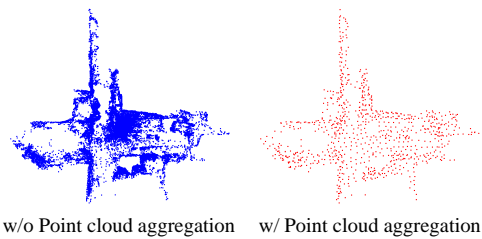


Figure 10. **Role of point aggregation.** We visualize the point distribution before and after the point aggregation. Our point aggregation module obtains a more uniform-distributed point set to fairly estimate the transformation matrix \mathbf{T} that achieves better 3D scene stylization results.

v , we warp the results generated at another novel view v' to the view v according to the 3D proxy geometry described in Section 3.1. We then compute the score by

$$E_{\text{warp}}(\mathbf{O}_v, \mathbf{O}'_v) = \text{LPIPS}(\mathbf{O}_v, W(\mathbf{O}'_v), \mathbf{M}_{v'v}), \quad (3)$$

where W is the warping function and $\mathbf{M}_{v'v}$ is the mask of valid pixels warped from the views v' to v . Note that we only use the values of valid pixels in the mask for the “spatial average” operation in [114]. For each of the testing scenes in the Tanks and Temples dataset, we use 15 style images [20] to compute the average warping error.

We first present the short-range consistency comparison in Table 1. In this experiment, we use the nearby view for a specific novel view to compute the warping error.¹ In general, the image stylization alternative methods produce short-range inconsistent results as they process each novel view independently. In contrast, the proposed method performs comparably against the video stylization-based approach SVS→Compound that considers the short-term consistency in videos. Nevertheless, SVS→Compound synthesizes bland styles that do not match the desired styles, as the results demonstrated in Figure 6 and Figure 8.

Long-range consistency. We also consider the long-range

¹We use the viewpoints of $(t - 1)$ -th and t -th testing video frames as the views v' and v , respectively.

consistency issue in our experiments. In this experiment, we compute the warping error between the results of two (relatively) far-away views.² As demonstrated in Table 2, the proposed method performs favorably against the alternative approaches. Despite the capability of ensuring short-range consistency, video stylization-based schemes fail to maintain the long-range consistency.

Number of point cloud aggregation modules. We conduct an ablation study to decide the number of point cloud aggregation modules described in Section 3.2. The results are presented in Figure 9. We empirically choose to use three modules for better visual quality. Moreover, we visualize the point distributions before and after the aggregation in Figure 10 to understand the role of the aggregation module. The point density before the aggregation is higher around the regions of the 3D scene where more input images cover. As a result, the prediction of the transformation matrix \mathbf{T} is dominated by such regions, which leads to low-quality stylization results (2nd column in Figure 9). By using the point cloud aggregation modules, we obtain a more uniform-distributed point set that fairly estimates the matrix \mathbf{T} for the 3D scene stylization task.

5. Conclusions

In this work, we introduce a 3D scene stylization problem that aims to modify the style of the 3D scene and synthesize images at arbitrary novel views. We construct a single 3D representation, *i.e.* point cloud, for the holistic scene, and design a point cloud transformation module to transfer the style of the reference image to the 3D representation. Qualitative and quantitative evaluations validate that our method synthesizes images that 1) contain the desired style and 2) are consistent across various novel views.

Acknowledgements

This work is supported in part by the NSF CAREER Grant #1149783 and a gift from Verisk.

²We use the viewpoints of $(t - 7)$ -th and t -th testing video frames as the views v' and v , respectively.

References

- [1] Kara-Ali Aliev, Artem Sevastopolsky, Maria Kolos, Dmitry Ulyanov, and Victor Lempitsky. Neural point-based graphics. In *ECCV*, 2020. 2
- [2] Iro Armeni, Sasha Sax, Amir R Zamir, and Silvio Savarese. Joint 2d-3d-semantic data for indoor scene understanding. *arXiv preprint arXiv:1702.01105*, 2017. 3
- [3] Jonathan T. Barron, Ben Mildenhall, Matthew Tancik, Peter Hedman, Ricardo Martin-Brualla, and Pratul P. Srinivasan. Mip-nerf: A multiscale representation for anti-aliasing neural radiance fields. In *ICCV*, 2021. 17
- [4] Mark Boss, Raphael Braun, Varun Jampani, Jonathan T. Barron, Ce Liu, and Hendrik P.A. Lensch. Nerf: Neural reflectance decomposition from image collections. *arXiv preprint arXiv:2012.03918*, 2020. 17
- [5] Xu Cao, Weimin Wang, Katashi Nagao, and Ryosuke Nakamura. Psnet: A style transfer network for point cloud stylization on geometry and color. In *WACV*, 2020. 3, 15, 16
- [6] Eric Chan, Marco Monteiro, Petr Kellnhofer, Jiajun Wu, and Gordon Wetzstein. pi-gan: Periodic implicit generative adversarial networks for 3d-aware image synthesis. In *CVPR*, 2021. 17
- [7] Anpei Chen, Zexiang Xu, Fuqiang Zhao, Xiaoshuai Zhang, Fanbo Xiang, Jingyi Yu, and Hao Su. MVSNeRF: Fast Generalizable Radiance Field Reconstruction from Multi-View Stereo. In *ICCV*, 2021. 17
- [8] Dongdong Chen, Jing Liao, Lu Yuan, Nenghai Yu, and Gang Hua. Coherent online video style transfer. In *ICCV*, 2017. 3
- [9] Dongdong Chen, Lu Yuan, Jing Liao, Nenghai Yu, and Gang Hua. Stylebank: An explicit representation for neural image style transfer. In *CVPR*, 2017. 2
- [10] Dongdong Chen, Lu Yuan, Jing Liao, Nenghai Yu, and Gang Hua. Stereoscopic neural style transfer. In *CVPR*, 2018. 3
- [11] Xinghao Chen, Yiman Zhang, Yunhe Wang, Han Shu, Chunjing Xu, and Chang Xu. Optical flow distillation: Towards efficient and stable video style transfer. In *ECCV*, 2020. 3
- [12] Jia Deng, Wei Dong, Richard Socher, Li-Jia Li, Kai Li, and Li Fei-Fei. Imagenet: A large-scale hierarchical image database. In *CVPR*, 2009. 4
- [13] Kangle Deng, Andrew Liu, Jun-Yan Zhu, and Deva Ramanan. Depth-supervised nerf: Fewer views and faster training for free. *arXiv preprint arXiv:2107.02791*, 2021. 17
- [14] Yingying Deng, Fan Tang, Weiming Dong, haibin Huang, Ma chongyang, and Changsheng Xu. Arbitrary video style transfer via multi-channel correlation. In *AAAI*, 2021. 2, 3, 6
- [15] Terrance DeVries, Miguel Angel Bautista, Nitish Srivastava, Graham W. Taylor, and Joshua M. Susskind. Unconstrained scene generation with locally conditioned radiance fields. In *ICCV*, 2021. 17
- [16] Yilun Du, Yanan Zhang, Hong-Xing Yu, Joshua B. Tenenbaum, and Jiajun Wu. Neural radiance flow for 4d view synthesis and video processing. In *ICCV*, 2021. 17
- [17] Guy Gafni, Justus Thies, Michael Zollhöfer, and Matthias Nießner. Dynamic neural radiance fields for monocular 4d facial avatar reconstruction. In *CVPR*, 2021. 17
- [18] Chang Gao, Derun Gu, Fangjun Zhang, and Y. Yu. Reconet: Real-time coherent video style transfer network. In *ACCV*, 2018. 3
- [19] Chen Gao, Yichang Shih, Wei-Sheng Lai, Chia-Kai Liang, and Jia-Bin Huang. Portrait neural radiance fields from a single image. *arXiv preprint arXiv:2012.05903*, 2020. 17
- [20] Wei Gao, Yijun Li, Yihang Yin, and Ming-Hsuan Yang. Fast video multi-style transfer. In *WACV*, 2020. 2, 3, 6, 8
- [21] Stephan J Garbin, Marek Kowalski, Matthew Johnson, Jamie Shotton, and Julien Valentin. Fastnerf: High-fidelity neural rendering at 200fps. *arXiv preprint arXiv:2103.10380*, 2021. 17
- [22] Leon A. Gatys, Alexander S. Ecker, and Matthias Bethge. Image style transfer using convolutional neural networks. In *CVPR*, 2016. 2
- [23] Xinyu Gong, Haozhi Huang, Lin Ma, Fumin Shen, Wei Liu, and Tong Zhang. Neural stereoscopic image style transfer. In *ECCV*, 2018. 3
- [24] Teofilo F Gonzalez. Clustering to minimize the maximum intercluster distance. *Theoretical computer science*, 38:293–306, 1985. 4
- [25] Michelle Guo, Alireza Fathi, Jiajun Wu, and Thomas Funkhouser. Object-centric neural scene rendering. *arXiv preprint arXiv:2012.08503*, 2020. 17
- [26] Agrim Gupta, Justin Johnson, Alexandre Alahi, and Li Fei-Fei. Characterizing and improving stability in neural style transfer. In *ICCV*, 2017. 3
- [27] Tewodros Habtegebrail, Varun Jampani, Orazio Gallo, and Didier Stricker. Generative view synthesis: From single-view semantics to novel-view images. In *NeurIPS*, 2020. 1
- [28] David Hart, Bryan Morse, and Jessica Greenland. Style transfer for light field photography. In *WACV*, 2020. 3
- [29] Haozhi Huang, Hao Wang, Wenhan Luo, Lin Ma, Wenhao Jiang, Xiaolong Zhu, Zhifeng Li, and Wei Liu. Real-time neural style transfer for videos. In *CVPR*, 2017. 3
- [30] Hsin-Ping Huang, Hung-Yu Tseng, Hsin-Ying Lee, and Jia-Bin Huang. Semantic view synthesis. In *ECCV*, 2020. 1
- [31] Xun Huang and Serge Belongie. Arbitrary style transfer in real-time with adaptive instance normalization. In *ICCV*, 2017. 3
- [32] Michal Jancosek and Tomas Pajdla. Multi-view reconstruction preserving weakly-supported surfaces. In *CVPR*, 2011. 4
- [33] Justin Johnson, Alexandre Alahi, and Li Fei-Fei. Perceptual losses for real-time style transfer and super-resolution. In *ECCV*, 2016. 2, 6
- [34] Hiroharu Kato, Yoshitaka Ushiku, and Tatsuya Harada. Neural 3d mesh renderer. In *CVPR*, 2018. 3
- [35] Diederik Kingma and Jimmy Ba. Adam: A method for stochastic optimization. In *ICLR*, 2015. 17
- [36] Roman Klokov and Victor Lempitsky. Escape from cells: Deep kd-networks for the recognition of 3d point cloud models. In *ICCV*, 2017. 3
- [37] Arno Knapitsch, Jaesik Park, Qian-Yi Zhou, and Vladlen Koltun. Tanks and temples: Benchmarking large-scale scene reconstruction. *ACM TOG (Proc. SIGGRAPH)*, 36(4), 2017. 2, 3, 5, 6, 7, 13, 15

- [38] Johannes Kopf, Michael Cohen, and Richard Szeliski. First-person hyper-lapse videos. *ACM TOG (Proc. SIGGRAPH)*, 33:1–10, 07 2014. 4
- [39] Johannes Kopf, Kevin Matzen, Suhub Alsisan, Ocean Quigley, Francis Ge, Yangming Chong, Josh Patterson, Jan-Michael Frahm, Shu Wu, Matthew Yu, et al. One shot 3d photography. *ACM TOG (Proc. SIGGRAPH)*, 39(4):76–1, 2020. 2
- [40] Adam R. Kosiorok, Heiko Strathmann, Daniel Zoran, Pol Moreno, Rosalia Schneider, Soňa Mokrá, and Danilo J. Rezende. Nerf-vae: A geometry aware 3d scene generative model. In *ICML*, 2021. 17
- [41] Truc Le and Ye Duan. Pointgrid: A deep network for 3d shape understanding. In *CVPR*, 2018. 3
- [42] Jiaxin Li, Ben M Chen, and Gim Hee Lee. So-net: Self-organizing network for point cloud analysis. In *CVPR*, 2018. 3
- [43] Tianye Li, Mira Slavcheva, M. Zollhöfer, S. Green, Christoph Lassner, Changil Kim, Tanner Schmidt, S. Lovegrove, M. Goesele, and Z. Lv. Neural 3d video synthesis. *arXiv preprint arXiv:2103.02597*, 2021. 17
- [44] Xueting Li, Sifei Liu, Jan Kautz, and Ming-Hsuan Yang. Learning linear transformations for fast arbitrary style transfer. In *CVPR*, 2019. 1, 2, 3, 4, 6, 13
- [45] Yangyan Li, Rui Bu, Mingchao Sun, Wei Wu, Xinhan Di, and Baoquan Chen. Pointcnn: Convolution on x-transformed points. In *NIPS*, 2018. 3
- [46] Yijun Li, Chen Fang, Jimei Yang, Zhaowen Wang, Xin Lu, and Ming-Hsuan Yang. Diversified texture synthesis with feed-forward networks. In *CVPR*, 2017. 2
- [47] Yijun Li, Chen Fang, Jimei Yang, Zhaowen Wang, Xin Lu, and Ming-Hsuan Yang. Universal style transfer via feature transforms. In *NIPS*, 2017. 3, 17
- [48] Zhengqi Li, Simon Niklaus, Noah Snavely, and Oliver Wang. Neural scene flow fields for space-time view synthesis of dynamic scenes. In *CVPR*, 2021. 17
- [49] David B. Lindell, Julien N. P. Martel, and Gordon Wetstein. Autoint: Automatic integration for fast neural volume rendering. In *CVPR*, 2021. 17
- [50] Andrew Liu, Richard Tucker, Varun Jampani, Ameesh Makadia, Noah Snavely, and Angjoo Kanazawa. Infinite nature: Perpetual view generation of natural scenes from a single image. *arXiv preprint arXiv:2012.09855*, 2020. 1
- [51] Lingjie Liu, Jiatao Gu, Kyaw Zaw Lin, Tat-Seng Chua, and Christian Theobalt. Neural sparse voxel fields. In *NeurIPS*, 2020. 2, 17
- [52] Steven Liu, Xiuming Zhang, Zhoutong Zhang, Richard Zhang, Jun-Yan Zhu, and Bryan Russell. Editing conditional radiance fields. *arXiv preprint arXiv:2105.06466*, 2021. 17
- [53] Stephen Lombardi, Tomas Simon, Gabriel Schwartz, Michael Zollhoefer, Yaser Sheikh, and Jason M. Saragih. Mixture of volumetric primitives for efficient neural rendering. *ACM TOG (Proc. SIGGRAPH)*, 40:1 – 13, 2021. 17
- [54] Arun Mallya, Ting-Chun Wang, Karan Sapra, and Ming-Yu Liu. World-consistent video-to-video synthesis. In *ECCV*, 2020. 3
- [55] Ricardo Martin-Brualla, Noha Radwan, Mehdi S. M. Sajjadi, Jonathan T. Barron, Alexey Dosovitskiy, and Daniel Duckworth. NeRF in the Wild: Neural Radiance Fields for Unconstrained Photo Collections. In *CVPR*, 2021. 17
- [56] Quan Meng, Anpei Chen, Haimin Luo, Minye Wu, Hao Su, Lan Xu, Xuming He, and Jingyi Yu. GNeRF: GAN-based Neural Radiance Field without Posed Camera. In *ICCV*, 2021. 17
- [57] Moustafa Meshry, Dan B. Goldman, Sameh Khamis, Hugues Hoppe, Rohit Pandey, Noah Snavely, and Ricardo Martin-Brualla. Neural re-rendering in the wild. In *CVPR*, 2019. 2
- [58] Ben Mildenhall, Pratul P. Srinivasan, Rodrigo Ortiz-Cayon, Nima Khademi Kalantari, Ravi Ramamoorthi, Ren Ng, and Abhishek Kar. Local light field fusion: Practical view synthesis with prescriptive sampling guidelines. *ACM TOG (Proc. SIGGRAPH)*, 38:1 – 14, 2019. 13
- [59] Ben Mildenhall, Pratul P Srinivasan, Matthew Tancik, Jonathan T Barron, Ravi Ramamoorthi, and Ren Ng. Nerf: Representing scenes as neural radiance fields for view synthesis. In *ECCV*, 2020. 1, 2, 17
- [60] Carsten Moenning and Neil A Dodgson. Fast marching farthest point sampling. Technical report, University of Cambridge, Computer Laboratory, 2003. 4
- [61] Thomas Neff, Pascal Stadlbauer, Mathias Parger, Andreas Kurz, Joerg H. Mueller, Chakravarty R. Alla Chaitanya, Anton S. Kaplanyan, and Markus Steinberger. DONeRF: Towards Real-Time Rendering of Compact Neural Radiance Fields using Depth Oracle Networks. *Computer Graphics Forum*, 40(4), 2021. 17
- [62] Michael Niemeyer and Andreas Geiger. Campari: Camera-aware decomposed generative neural radiance fields. *arXiv preprint arXiv:2103.17269*, 2021. 17
- [63] Michael Niemeyer and Andreas Geiger. Giraffe: Representing scenes as compositional generative neural feature fields. In *CVPR*, 2021. 17
- [64] Simon Niklaus, Long Mai, Jimei Yang, and Feng Liu. 3d ken burns effect from a single image. *ACM TOG (Proc. SIGGRAPH)*, 38(6):1–15, 2019. 2
- [65] Atsuhiko Noguchi, Xiao Sun, Stephen Lin, and Tatsuya Harada. Neural articulated radiance field. *arXiv preprint arXiv:2104.03110*, 2021. 17
- [66] Julian Ost, Fahim Mannan, Nils Thuerey, Julian Knodt, and Felix Heide. Neural scene graphs for dynamic scenes. In *CVPR*, 2021. 17
- [67] Keunhong Park, Utkarsh Sinha, Jonathan T. Barron, Sofien Bouaziz, Dan B Goldman, Steven M. Seitz, and Ricardo Martin-Brualla. Deformable neural radiance fields. In *ICCV*, 2021. 17
- [68] Keunhong Park, Utkarsh Sinha, Peter Hedman, Jonathan T. Barron, Sofien Bouaziz, Dan B Goldman, Ricardo Martin-Brualla, and Steven M. Seitz. Hypernerf: A higher-dimensional representation for topologically varying neural radiance fields. *arXiv preprint arXiv:2106.13228*, 2021. 17
- [69] Sida Peng, Junting Dong, Qianqian Wang, Shangzhan Zhang, Qing Shuai, Hujun Bao, and Xiaowei Zhou. Animatable neural radiance fields for human body modeling. In *ICCV*, 2021. 17
- [70] Sida Peng, Yuanqing Zhang, Yinghao Xu, Qianqian Wang, Qing Shuai, Hujun Bao, and Xiaowei Zhou. Neural body:

- Implicit neural representations with structured latent codes for novel view synthesis of dynamic humans. In *CVPR*, 2021. 17
- [71] Albert Pumarola, Enric Corona, Gerard Pons-Moll, and Francesc Moreno-Noguer. D-nerf: Neural radiance fields for dynamic scenes. In *CVPR*, 2021. 17
- [72] Charles R Qi, Hao Su, Kaichun Mo, and Leonidas J Guibas. Pointnet: Deep learning on point sets for 3d classification and segmentation. In *CVPR*, 2017. 3
- [73] Charles Ruizhongtai Qi, Li Yi, Hao Su, and Leonidas J Guibas. Pointnet++: Deep hierarchical feature learning on point sets in a metric space. In *NIPS*, 2017. 3
- [74] Charles R Qi, Li Yi, Hao Su, and Leonidas J Guibas. Pointnet++: Deep hierarchical feature learning on point sets in a metric space. In *NIPS*, 2017. 4
- [75] Amit Raj, Michael Zollhoefer, Tomas Simon, Jason Saragih, Shunsuke Saito, James Hays, and Stephen Lombardi. Pva: Pixel-aligned volumetric avatars. In *CVPR*, 2021. 17
- [76] Nikhila Ravi, Jeremy Reizenstein, David Novotny, Taylor Gordon, Wan-Yen Lo, Justin Johnson, and Georgia Gkioxari. Accelerating 3d deep learning with pytorch3d. *arXiv preprint arXiv:2007.08501*, 2020. 4, 16
- [77] Daniel Rebain, Wei Jiang, Soroosh Yazdani, Ke Li, Kwang Moo Yi, and Andrea Tagliasacchi. Derf: Decomposed radiance fields. In *CVPR*, 2021. 17
- [78] Christian Reiser, Songyou Peng, Yiyi Liao, and Andreas Geiger. Kilonerf: Speeding up neural radiance fields with thousands of tiny mlps. In *ICCV*, 2021. 17
- [79] Konstantinos Rematas, Ricardo Martin-Brualla, and Vittorio Ferrari. Sharf: Shape-conditioned radiance fields from a single view. In *ICML*, 2021. 17
- [80] Gernot Riegler and Vladlen Koltun. Free view synthesis. In *ECCV*, 2020. 2, 6
- [81] Gernot Riegler and Vladlen Koltun. Stable view synthesis. In *CVPR*, 2021. 1, 2, 6, 13
- [82] Johannes L. Schonberger and Jan-Michael Frahm. Structure-from-motion revisited. In *CVPR*, 2016. 4
- [83] Katja Schwarz, Yiyi Liao, Michael Niemeyer, and Andreas Geiger. Graf: Generative radiance fields for 3d-aware image synthesis. In *NeurIPS*, 2020. 17
- [84] Johannes Schönberger, Enliang Zheng, Marc Pollefeys, and Jan-Michael Frahm. Pixelwise view selection for unstructured multi-view stereo. In *ECCV*, 2016. 4
- [85] Falong Shen, Shuicheng Yan, and Gang Zeng. Neural style transfer via meta networks. In *CVPR*, 2018. 2
- [86] Meng-Li Shih, Shih-Yang Su, Johannes Kopf, and Jia-Bin Huang. 3d photography using context-aware layered depth inpainting. In *CVPR*, 2020. 2
- [87] Karen Simonyan and Andrew Zisserman. Very deep convolutional networks for large-scale image recognition. In *ICLR*, 2015. 4, 13
- [88] Pratul P. Srinivasan, Boyang Deng, Xiuming Zhang, Matthew Tancik, Ben Mildenhall, and Jonathan T. Barron. Nerv: Neural reflectance and visibility fields for relighting and view synthesis. In *CVPR*, 2021. 17
- [89] Pratul P. Srinivasan, Richard Tucker, Jonathan T. Barron, Ravi Ramamoorthi, Ren Ng, and Noah Snavely. Pushing the boundaries of view extrapolation with multiplane images. In *CVPR*, 2019. 2
- [90] Shih-Yang Su, Frank Yu, Michael Zollhoefer, and Helge Rhodin. A-nerf: Surface-free human 3d pose refinement via neural rendering. *arXiv preprint arXiv:2102.06199*, 2021. 17
- [91] Edgar Sucar, Shikun Liu, Joseph Ortiz, and Andrew Davidson. iMAP: Implicit mapping and positioning in real-time. *arXiv preprint arXiv:2103.12352*, 2021. 17
- [92] Jan Svoboda, Asha Anoopsh, Christian Osendorfer, and Jonathan Masci. Two-stage peer-regularized feature recombination for arbitrary image style transfer. In *CVPR*, 2020. 1, 3, 6
- [93] Matthew Tancik, Ben Mildenhall, Terrance Wang, Divi Schmidt, Pratul P. Srinivasan, Jonathan T. Barron, and Ren Ng. Learned initializations for optimizing coordinate-based neural representations. In *CVPR*, 2021. 17
- [94] Edgar Tretschk, Ayush Tewari, Vladislav Golyanik, Michael Zollhöfer, Christoph Lassner, and Christian Theobalt. Non-rigid neural radiance fields: Reconstruction and novel view synthesis of a deforming scene from monocular video. In *ICCV*, 2021. 17
- [95] Alex Trevithick and Bo Yang. Grf: Learning a general radiance field for 3d scene representation and rendering. *arXiv preprint arXiv:2010.04595*, 2020. 17
- [96] Richard Tucker and Noah Snavely. Single-view view synthesis with multiplane images. In *CVPR*, 2020. 2
- [97] Dmitry Ulyanov, Vadim Lebedev, Andrea Vedaldi, and Victor Lempitsky. Texture networks: Feed-forward synthesis of textures and stylized images. In *ICML*, 2016. 2
- [98] Qianqian Wang, Zhicheng Wang, Kyle Genova, Pratul Srinivasan, Howard Zhou, Jonathan T. Barron, Ricardo Martin-Brualla, Noah Snavely, and Thomas Funkhouser. Ibrnet: Learning multi-view image-based rendering. In *CVPR*, 2021. 17
- [99] Wenjing Wang, Jizheng Xu, Li Zhang, Yue Wang, and Jiaying Liu. Consistent video style transfer via compound regularization. In *AAAI*, 2020. 2, 3, 6
- [100] Ziyang Wang, Timur Bagautdinov, Stephen Lombardi, Tomas Simon, Jason Saragih, Jessica Hodgins, and Michael Zollhöfer. Learning compositional radiance fields of dynamic human heads. In *CVPR*, 2021. 17
- [101] Zirui Wang, Shangzhe Wu, Weidi Xie, Min Chen, and Victor Adrian Prisacariu. NeRF—: Neural radiance fields without known camera parameters. *arXiv preprint arXiv:2102.07064*, 2021. 17
- [102] Olivia Wiles, Georgia Gkioxari, Richard Szeliski, and Justin Johnson. SynSin: End-to-end view synthesis from a single image. In *CVPR*, 2020. 2, 4
- [103] Suttisak Wizadwongsa, Pakkapon Phongthawee, Jiraphon Yenphraphai, and Supasorn Suwajanakorn. Nex: Real-time view synthesis with neural basis expansion. In *CVPR*, 2021. 2, 13, 17
- [104] Wenxuan Wu, Zhongang Qi, and Li Fuxin. Pointconv: Deep convolutional networks on 3d point clouds. In *CVPR*, 2019. 3
- [105] Zhirong Wu, Shuran Song, Aditya Khosla, Fisher Yu, Linguang Zhang, Xiaoou Tang, and Jianxiong Xiao. 3d shapenets: A deep representation for volumetric shapes. In *CVPR*, 2015. 3

- [106] Wenqi Xian, Jia-Bin Huang, Johannes Kopf, and Changil Kim. Space-time neural irradiance fields for free-viewpoint video. In *CVPR*, 2021. [17](#)
- [107] Christopher Xie, Keunhong Park, Ricardo Martin-Brualla, and Matthew Brown. Fig-nerf: Figure-ground neural radiance fields for 3d object category modelling. *arXiv preprint arXiv:2104.08418*, 2021. [17](#)
- [108] Saining Xie, Sainan Liu, Zeyu Chen, and Zhuowen Tu. Attentional shapecontextnet for point cloud recognition. In *CVPR*, 2018. [3](#)
- [109] Lin Yen-Chen, Pete Florence, Jonathan T. Barron, Alberto Rodriguez, Phillip Isola, and Tsung-Yi Lin. iNeRF: Inverting neural radiance fields for pose estimation. In *IROS*, 2021. [17](#)
- [110] Li Yi, Vladimir G Kim, Duygu Ceylan, I-Chao Shen, Mengyan Yan, Hao Su, Cewu Lu, Qixing Huang, Alla Sheffer, and Leonidas Guibas. A scalable active framework for region annotation in 3d shape collections. *ACM TOG (Proc. SIGGRAPH)*, 35(6):1–12, 2016. [3](#)
- [111] Alex Yu, Ruilong Li, Matthew Tancik, Hao Li, Ren Ng, and Angjoo Kanazawa. Plenotrees for real-time rendering of neural radiance fields. In *ICCV*, 2021. [17](#)
- [112] Alex Yu, Vickie Ye, Matthew Tancik, and Angjoo Kanazawa. pixelNeRF: Neural radiance fields from one or few images. In *CVPR*, 2021. [2](#), [17](#)
- [113] Kai Zhang, Gernot Riegler, Noah Snavely, and Vladlen Koltun. Nerf++: Analyzing and improving neural radiance fields. *arXiv preprint arXiv:2010.07492*, 2020. [1](#), [2](#), [6](#), [13](#), [17](#)
- [114] Richard Zhang, Phillip Isola, Alexei A Efros, Eli Shechtman, and Oliver Wang. The unreasonable effectiveness of deep features as a perceptual metric. In *CVPR*, 2018. [2](#), [7](#), [8](#)
- [115] Xiuming Zhang, Pratul P Srinivasan, Boyang Deng, Paul Debevec, William T Freeman, and Jonathan T Barron. NeRFactor: Neural Factorization of Shape and Reflectance Under an Unknown Illumination. *ACM TOG (Proc. SIGGRAPH Asia)*, 2021. [17](#)
- [116] Hengshuang Zhao, Li Jiang, Chi-Wing Fu, and Jiaya Jia. PointWeb: Enhancing local neighborhood features for point cloud processing. In *CVPR*, 2019. [3](#)
- [117] Shuaifeng Zhi, Tristan Laidlow, Stefan Leutenegger, and Andrew Davison. In-place scene labelling and understanding with implicit scene representation. In *ICCV*, 2021. [17](#)
- [118] Tinghui Zhou, Richard Tucker, John Flynn, Graham Fyffe, and Noah Snavely. Stereo magnification: learning view synthesis using multiplane images. *ACM TOG (Proc. SIGGRAPH)*, 37(4):1–12, 2018. [2](#)

A. Supplementary Materials

A.1. Overview

In this supplementary document, we first present additional experimental results, including run-time analysis. Second, we provide the implementation details of the proposed framework. Third, we compare our method (*i.e.* explicit representations) and the current approaches based on implicit representations. Finally, we discuss the limitations of the proposed scheme and the future research directions. More qualitative comparisons are available at https://hhsinping.github.io/3d_scene_stylization.

A.2. Additional Experimental Results

A.2.1 LLFF and Shiny datasets

To demonstrate the generalization ability of the proposed method, we use the model trained on the Tanks and Temples dataset [37] to produce the stylization results on two additional datasets: LLFF [58] and Shiny [103].



Figure 11. **Additional results.** We show additional results on LLFF and Shiny datasets using the model trained on the Tanks and Temples dataset.

A.2.2 LST→NeRF++

As shown in Figure 5 in the paper, applying image stylization schemes before the SVS [81] framework produces blurry results. In this experiment, we show that replacing the SVS [81] with NeRF++ [113] approaches suffers from the similar issue. In Figure 12, we present the results LST [44] → NeRF++ [113]. Since the input images are not consistent due to the per-image stylization by the LST approach, the NeRF++ model tends to *blend* such inconsistency, which leads to blurry results.



Figure 12. **LST→NeRF++.** The NeRF++ approach produces blurry results if the input images are not consistent due to the per-image stylization by the LST approach.

A.2.3 Ablation Study on Stylization Level

We use the pre-trained VGG-19 model [87] to extract the feature of the input images for the point cloud construction. By extracting the features from different layers of the VGG-19 network, our point cloud representation encodes different levels of the style information. Figure 13 demonstrates that our framework is capable of transferring the different style levels.

Specifically, building the point cloud representation using the deeper (*e.g.* relu4_1) features produces more distortion, while using the shallower (*e.g.* relu3_1) features generates more photo-realistic (*i.e.* preserve more content information) effects.

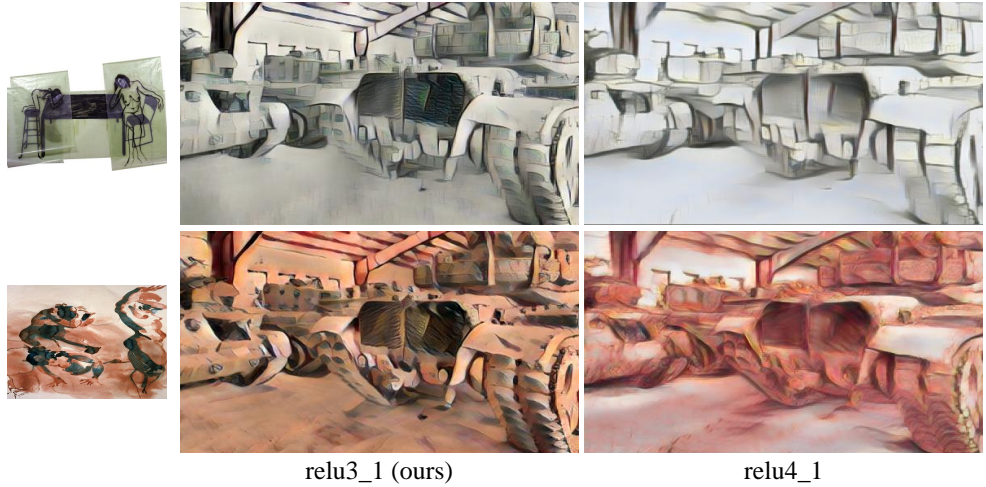


Figure 13. **Ablation study on stylization level.** We show that our framework is able to transfer styles of different levels. Extracting the image features from the deeper layers (relu4_1) of the pre-trained VGG-19 network produces more distortion, while using features from the shallower layers (relu3_1) generates more photo-realistic stylization effects.

A.2.4 Ablation Study on Point Cloud Aggregation

To gather the style information of the constructed point cloud $\{f_p^c\}_{p=1}^P$, we sample a subset of P' points $\{f_p^c\}_{p=1}^{P'}$ and then use a radius parameter r to find k nearby points to form a point group. Each point group is aggregated to a vector by MLP layers and the max pooling operator to form the aggregated point cloud $\{f_p^c\}_{p=1}^{P'}$. We conduct the following ablation studies to analyze the hyper-parameters r and k .

Radius r . Figure 14 shows the results of using different sets of radius parameters r for our point cloud aggregation modules. We empirically choose to use $r=\{0.05,0.1,0.2\}$ for better visual quality.

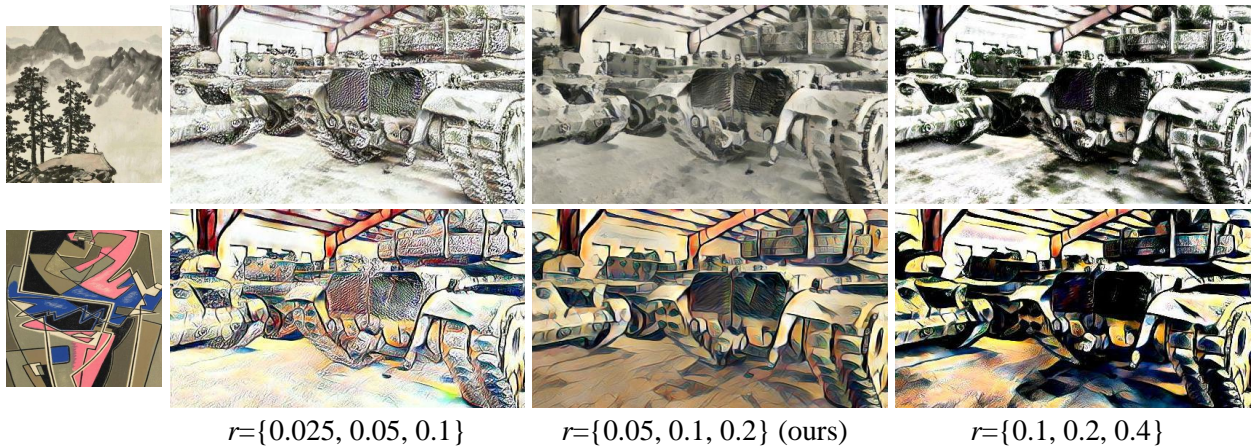


Figure 14. **Ablation study on hyper-parameter r in the point cloud aggregation.** We compare the visual results of setting $r = \{0.025, 0.05, 0.1\}$, $r = \{0.05, 0.1, 0.2\}$, $r = \{0.1, 0.2, 0.4\}$. We empirically determine to use $r = \{0.05, 0.1, 0.2\}$ for better visual quality.

Number of sampled points k . We conduct an ablation study to decide the parameter k . Figure 15 shows the results of setting $k = 32/64/128$. We found that increasing the value of k produces results with higher contrast. We set $k=64$ since the results better match the style of the reference image.

Quantitative analysis of applying point cloud aggregation modules. In Table 3, we provide the quantitative analysis to understand the impact of applying the point cloud aggregation modules on the consistency issue. The results validate that



Figure 15. **Ablation study on hyper-parameter k in the point cloud aggregation.** We compare the visual results of using $k = 32/64/128$, and empirically choose to use $k = 64$ for better visual quality.

using point aggregation modules improves both short-range and long-range consistency.

Table 3. **Ablation study on point cloud aggregation.** We compute the short-range and long-range warping errors of the results generated by models with and without the point aggregation modules. We validate that applying the point aggregation modules achieves better consistency across various novel views.

(a) Short-range consistency					
Method	Truck	Playground	Train	M60	Average
w/ aggregation	0.182	0.150	0.166	0.164	0.165
w/o aggregation	0.187	0.159	0.167	0.164	0.168
(b) Long-range consistency					
Method	Truck	Playground	Train	M60	Average
w/ aggregation	0.590	0.332	0.409	0.434	0.428
w/o aggregation	0.595	0.374	0.417	0.409	0.434

A.2.5 PSNet for 3D Scene Stylization

The PSNet [5] model aims to transfer the style of the point cloud. However, it is not applicable to our problem for two reasons. First, PSNet requires per scene optimization on the “RGB” point cloud. It fails to handle large-scale scenes in the real-world with more than 60M points, such as those in the Tanks and Temples dataset [37]. To make the PSNet framework applicable to our problem, we first use uniform sampling to reduce the number of RGB points in the point cloud to 1M, then run PSNet framework to stylize the point cloud. We conduct the optimization process for the M60 and Truck scenes with 5000 iterations, which takes around 30 minutes for one specific combination of a scene and a reference image with desired style. Compared to the runtime of the proposed method shown in Table 4, the PSNet approach is time-consuming, thus limited for real-world applications. After the construction of the RGB point cloud, we project the points to the 2D image plane to synthesize images at novel views. As shown in Figure 16, we observe that PSNet does not generate desired stylization effect that matches the input reference image. In addition, the PSNet produces projection artifacts that require post-processing schemes (*e.g.* in-painting, smoothing) to refine the novel view synthesis results.

A.2.6 Runtime Analysis

In Table 4, we show the training and inference time of the proposed method. All the processes are conducted on a desktop machine equipped with a Nvidia Titan Xp GPU. We note that after the point cloud transformation (3rd row) is completed, we can synthesize novel view images in near-real-time (*i.e.* 17 fps).

A.3. Implementation Details

Network architecture. In Figure 17, we present the detailed architecture of each component in Figure 4 in the paper. We present the decoder architecture in Figure 18.



Figure 16. **3D scene stylization results of PSNet.** The PSNet [5] generates projection artifacts and fails to produce desired stylization effect that matches the input reference image.

Table 4. **Run-time analysis.** We present the training and inference time of each stage in the proposed method.

Training time: decoder (seconds / per iteration)	0.31
Training time: point cloud transformation module (seconds / per iteration)	1.78
Inference time: constructing point cloud (seconds / per input image)	0.21
Inference time: stylizing point cloud (seconds / per scene)	0.74
Inference time: rendering novel view (seconds / per view)	0.06

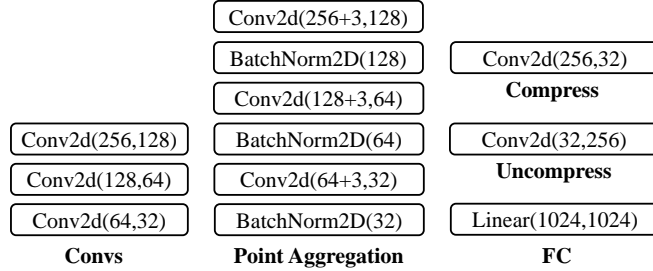


Figure 17. **Network architecture.** We present the network architecture of our point cloud transformation module illustrated in Figure 4 in the paper.

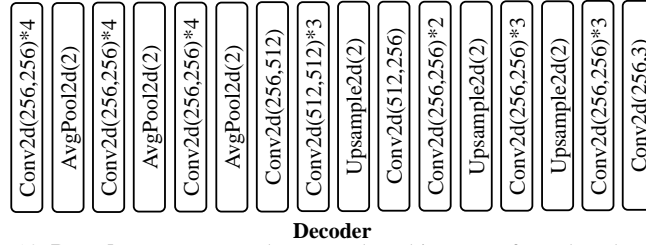


Figure 18. **Decoder.** We present the network architecture of our decoder module.

Point cloud transformation. To reduce the computation cost in our point cloud transformation step, we employ the *compress* and *uncompress* operations in practice, described as follows. The key is to reduce the feature dimension to accelerate the computation of the transformation matrix \mathbf{T} . Specifically, we reduce (*i.e.* compress) the feature dimension ($256 \rightarrow 32$) in the constructed point cloud $\{f_p^c\}_{p=1}^P$ through a MLP layer. We then transform the constructed point cloud $\{f_p^c\}_{p=1}^P$ using the transformation matrix \mathbf{T} of size 32×32 . Finally, we use a MLP layer to recover (*i.e.* uncompress) the feature dimension ($32 \rightarrow 256$) to produce the transformed point cloud $\{f_p^d\}_{p=1}^P$ for the following novel view synthesis stage. The process can be formulated as

$$f_p^d = \text{uncompress}(\mathbf{T}(\text{compress}(f_p^c - \bar{f}^c))) + \bar{f}^s \quad \forall p \in [1, \dots, P], \quad (4)$$

where \bar{f}^c is the mean of the features in the point cloud $\{f_p^c\}_{p=1}^P$, and \bar{f}^s is the mean of the style feature map \mathbf{F}^s .

Point cloud aggregation. The number of points P and feature dimension c in each point cloud aggregation module is $\{P, c\} : \{\approx 2M, 256\} \rightarrow \{4096, 128\} \rightarrow \{2048, 64\} \rightarrow \{1024, 32\}$.

Novel view synthesis. Given a novel view v with the camera pose $\{\mathbf{R}_v, t_v\}$ and intrinsic \mathbf{K}_v , we first project the features in our point cloud to the 2D image plane. Specifically, we use the Pytorch3D [76] point cloud renderer for the projection of features. We set the size of the z-buffer as 128 and the points are splatted to a region with radius of 2 pixels. We then use a decoder presented in Figure 18 to synthesize the final image from the projected 2D feature map.

Training. We implement our system in PyTorch, and use the Adam optimizer [35] with $\beta_1 = 0.9$, $\beta_2 = 0.9999$ for all network training. We first train the decoder module for 50K iterations with a batch size of 1 and learning rate of 0.0001. Following the WCT approach [47], the ℓ_1 reconstruction loss illustrated in Line 417 in the paper is the combination of the pixel reconstruction loss and feature loss. Particularly, the feature loss is computed using the features of a pre-trained VGG-19 network, including {conv1_2, conv2_2, conv3_2, conv4_2, conv5_2}. We then train the transformation module for 50K iterations with a batch size of 1 and learning rate of 0.0001. The content loss described in Eq. (2) in the paper is computed by the features of layer relu4_1, while the style loss is computed by {relu1_1, relu2_1, relu3_1, relu4_1}. The weight λ for the style loss is set to 0.02. To improve the training efficiency, we uniformly down-sample the constructed point cloud to 600K features for each scene, and use all the features in the point cloud during the testing time.

A.4. Explicit vs. Implicit Representations

While implicit representation-based approaches [3, 4, 6, 7, 13, 15, 16, 17, 19, 21, 25, 40, 43, 48, 49, 51, 52, 53, 55, 56, 59, 61, 62, 63, 65, 66, 67, 68, 69, 70, 71, 75, 77, 78, 79, 83, 88, 90, 91, 93, 94, 95, 98, 100, 101, 103, 106, 107, 109, 111, 112, 113, 115, 117] produce high-quality (non-stylized) novel view synthesis results, we choose to leverage explicit representations due to the practical considerations that support real-world VR/AR applications: *efficiency* and *scalability*. Specifically, the NeRF++ method [113] is designed for complex unbounded 3D scenes. Nevertheless, it takes 24 hours to reconstruct a *particular* scene, and 30 seconds to render a 546×980 image. Moreover, the NeRF++-based framework produces blurry stylization results due to the inconsistency issue, as shown in Figure 12. Although there are recent efforts [21, 49, 51, 53, 61, 77, 78, 111] to accelerate the rendering process, these schemes are limited to single 3D objects or bounded 3D scenes. In contrast, the proposed method is efficient, and renders the stylized novel views in near-real-time, as presented in Table 4. Furthermore, the proposed method is more scalable than the NeRF++-based approaches since it handles arbitrary unbounded scenes and styles with a single trained model.

A.5. Limitations and Future Direction

We discuss the limitation of our method, which we plan to explore in the future work as follows. First, as shown in Figure 19, our 3D scene stylization approach is not aware of the objects in the scene. As a result, we cannot transfer the style of the particular part of the style image to the specific object/region of the 3D scene. Second, the proposed approach cannot significantly modify the geometry of the scene during the stylization process since 1) our point cloud is built according to the 3D proxy of the original scene and 2) we only transform the features in our point cloud, but not adjust the location of each point. In the future, we plan to explore the solution that is 1) 3D object-aware and 2) capable of modulating the geometry of the 3D scene to match the desired style.



Figure 19. **Limitations.** Our model is not aware of individual objects in the scene during the stylization process, thus fail to transfer the style of a particular part of the reference image to the specific object/region in the scene.